ACS APPLIED MATERIALS & INTERFACES

Research Article

www.acsami.org

Electrochemical Post-Treatment of Infinite Coordination Polymers: An Effective Route to Preparation of Pd Nanoparticles Supported onto Carbon Nanotubes with Enhanced Electrocatalytic Activity toward Ethanol Oxidation

Lin Ren, Lifen Yang, Ping Yu, Yuexiang Wang, and Lanqun Mao*

Beijing National Laboratory for Molecular Sciences, Key Laboratory of Analytical Chemistry for Living Biosystems, Institute of Chemistry, Chinese Academy of Sciences, Beijing, 100190, China

ABSTRACT: This study describes an effective method to prepare highly dispersed palladium nanoparticles supported onto single-walled carbon nanotubes (SWNTs) with high electrocatalytic activity toward the oxidation of ethanol. This method is essentially based on electrochemical post-treatment of Pd-based infinite coordination polymer (ICP). The Pd-based ICP is synthesized through the coordination reaction between Zn^{2+} and metallo-Schiff base (MSB) to form Zn-MSB-Zn (ZMZ) ICP that precipitates from ethyl ether. The as-formed Zn-MSB-Zn ICP is then subjected to an ion-exchange reaction with Pd^{2+} to obtain the Zn-MSB-Pd (ZMP) ICP. To prepare Pd/SWNT nanocomposite, the ZMP ICP is mixed into the SWNT dispersion in *N*-dimethylformamide (DMF) to form a homogeneous dispersion that is then drop-coated onto a glassy carbon (GC) electrode. Electrochemical post-treatment of ZMP ICP to form Pd/SWNT nanocomposite is thus performed by polarizing the coated electrode at −0.2 V for 600 s in 0.5 M H_2SO_4. The results obtained with scanning electron microscopy (SEM) and transmission electron microscopy (TEM) reveal that the resulting Pd nanoparticles are highly dispersed onto SWNTs and the particles size are small and narrowly distributed (2.12 ± 0.32 nm). X-ray photoelectron spectroscopy (XPS) analysis shows that, after the electrochemical post-treatment, no detectable ZMP ICP precursors are left on the surface of SWNTs. The electrocatalytic activity of the as-formed Pd/SWNT nanocomposite toward ethanol oxidation is investigated by cyclic voltammetry and chronoamperometry. The results show that the Pd/SWNT nanocomposite prepared here shows a more negative potential and higher mass catalytic activity, as well as higher stability for the oxidation of ethanol than the commercial Pd/C catalyst. This work demonstrates a novel approach to the formation of ultrasmall and highly dispersed Pd/SWNT nanocomposite with enhanced electrocatalytic activity toward ethanol oxidation.

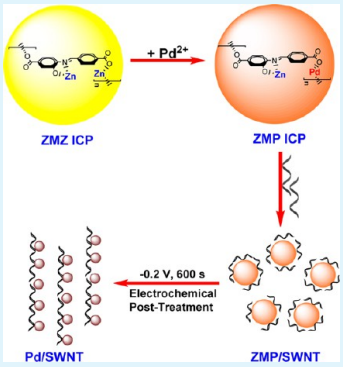

KEYWORDS: *palladium nanoparticles, electrochemical post-treatment, infinite coordination polymers, ethanol electrooxidation*

1. INTRODUCTION

Considerable efforts have been made on the design and formation of nonplatinum catalytic structures for direct alcohol fuel cells (DAFCs), in which carbon nanotubes-supported palladium nanoparticles are emerging as one of the most promising candidates. This is because Pd is more abundant in nature and less expensive than platinum, while is highly active for the oxidation of a large variety of substrates in alkaline environment.[1−7] Generally, to validate the application of Pd as an efficient catalyst for the alcohol oxidation in DAFCs, many factors have to be carefully considered, such as the size, morphology, shape, dispersion of Pd particles, as well as the nature of the supporting materials. All these factors play crucial roles in the electrocatalytic activity of Pd.[8−10] On the other hand, as one kind of carbon nanostructures with a high surface area, good electrical and thermal conductivity, carbon nanotubes have been demonstrated to be an excellent support for fuel cell electrocatalysts.[11,12] Early attempts have demonstrated that uniform dispersion, small size and narrow size distribution of Pd nanoparticles ensure excellent electrocatalytic activities of carbon nanotube supported Pd particles, yet the preparation of such kind of nanocomposites remains a challenge for most existing synthetic methods.[13−17] One of the difficulties lies in the ineffective adsorption of metal-salt precursors on the surface of carbon nanotubes because the surface of pristine nanotubes is relatively chemically inert.[18] The weak and uneven interactions between carbon nanotubes and metal-salt precursors unfortunately make it difficult to homogeneously disperse metal-salt precursors onto nanotubes, eventually resulting in the large size of Pd nanoparticles supported by nanotubes. To overcome this limitation, covalent or non-covalent functionalization of carbon nanotubes with, for example, organic acids, DNA, and polymers, in such a way that metal precursors can be attracted or effectively anchored onto the nanotube surface has been emerging as one of the most promising approaches.[13−17] However, the covalent

Received: September 16, 2013
Accepted: October 10, 2013
Published: October 10, 2013

Scheme 1. (A) Synthetic Routes of Zn-MSB-Pd Infinite Coordination Polymers (ZMP ICP) and (B) Illustration for the Formation of Pd/SWNT Nanocomposite by Electrochemical Post-Treatment of ZMP ICP at the Potential of −0.2 V in 0.5 M H_2SO_4

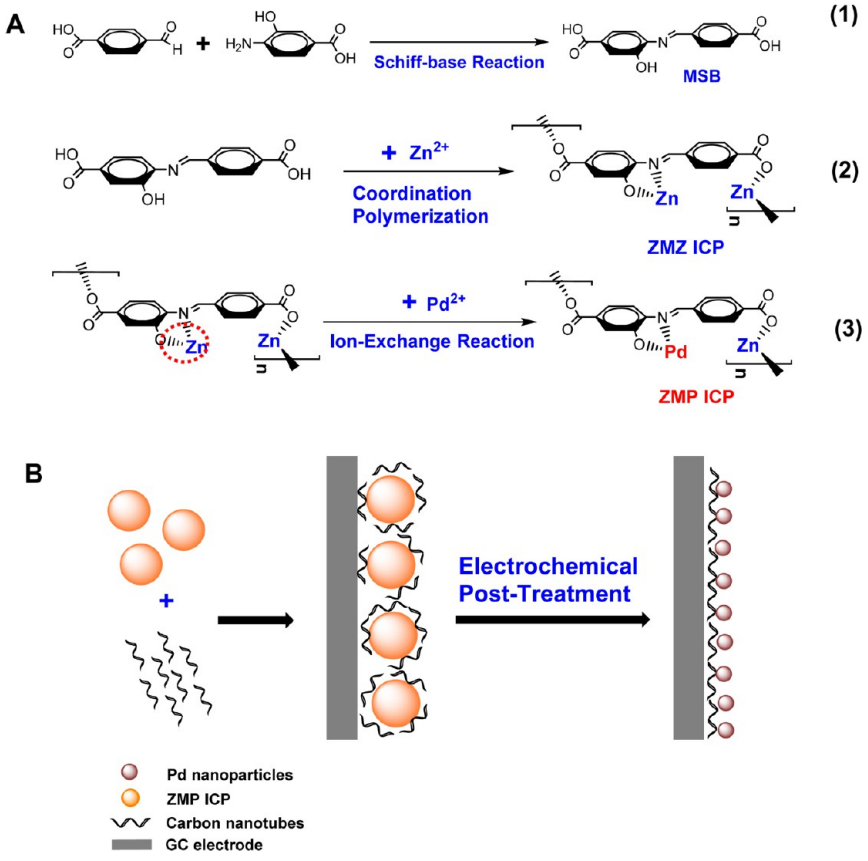

functionalization approaches generally cause severe damage to the structure of carbon nanotubes and thus greatly impair their physical and chemical properties, as reported previously.[1] The other difficulty lies in the fact that Pd nanoparticles spontaneously prefer to absorb and aggregate at the defects and the edges of the nanotubes during the deposition process, leading to a wide size distribution and difficulty in shape control of Pd nanoparticles. This problem could be solved by using protective reagents such as surfactants and ionic liquids to prevent aggregation of Pd nanoparticles.[19−22] However, the remaining of the protective reagents on the surface of Pd nanoparticles basically lowers the electrocatalytic activities of the as-synthesized nanostructures.[6] Although some methods have been reported to disperse Pd nanoparticles onto carbon nanotubes, a close examination reveals that these methods required either complex synthetic procedures or sophisticated equipment to obtain highly dispersed Pd nanoparticles with a small size and narrow size distribution.[23−25] As a consequence, a simple and stabilizer-free synthetic route to form ultrasmall and highly dispersed carbon nanotube-supported Pd nanocomposites with a high electrocatalytical performance is still highly desired.

In recent a few years, infinite coordination polymers (ICPs) have drawn a growing interest from both chemistry and material science because of their unique morphology and highly tailorable properties as well as promising applications.[26] ICPs can be conveniently synthesized in high yields through coordination chemistry with metal salts as central metal ions and multidentate organic or organometallic complexes as ligands. So far, the unique properties of ICPs have largely enabled their wide applications in many research fields such as catalysis, gas storage, separation, photonics and drug delivery.[27−31] More remarkably, recent efforts have demonstrated that post-treatment of ICPs could offer a new paradigm for the preparation of functional metal oxides and other kinds of nanostructures with tailorable size and morphology. For example, Oh and co-workers reported for the first time the synthesis of micrometer-sized ZnO hexagonal rings by calcination post-treatment of the amorphous hexagonal ring ICP particles at certain temperature.[32,33] By post-treating Cd(II)-glutathione (Cd-GSH) ICPs with alkaline, we have recently developed a novel method for green synthesis of CdS quantum dots with good water solubility and relatively high cytocompatibility.[34] In this study, we interestingly find that electrochemical post-treating Zn-MSB-Pd (ZMP) ICP essentially produces ultrasmall, narrowly size-distributed and highly dispersed carbon nanotube-supported Pd nanoparticles with an excellent electrocatalytic activity toward the electrooxidation of ethanol. The method demonstrated here is remarkable in the following aspects. (1) The electrochemical post-treatment strategy is stabilizer-free, technically simple yet relatively effective. (2) The as-synthesized Pd nanoparticles supported by single-walled carbon nanotubes (SWNTs) have an ultrasmall size with a narrow size distribution (2.12 ± 0.32 nm). (3) Since there is almost no Zn-MSB-Pd ICP precursor left on the as-deposited Pd nanoparticles after electrochemical post-treatment, the formed Pd/SWNT nanocomposite possesses a "clean" surface, which is believed to be beneficial to its

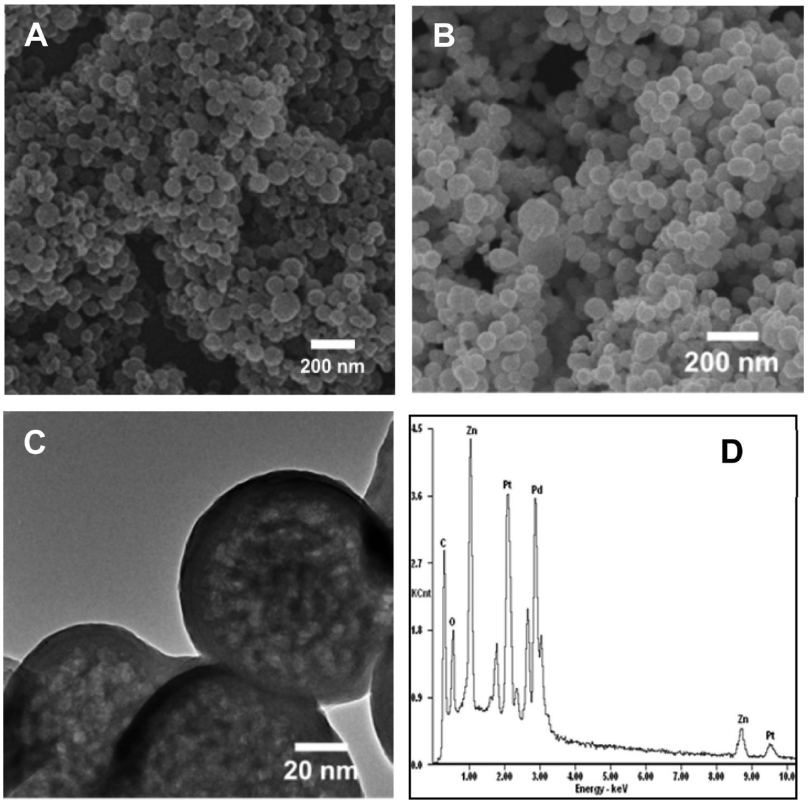

Figure 1. (A) SEM image of ZMZ ICP synthesized with coordination polymerization between MSB and $Zn(OAC)_2$ in DMSO. (B) SEM image, (C) TEM image and (D) EDX spetrum of ZMP ICP formed by an ion-exchange reaction between ZMZ ICP and $Pd(OAC)_2$ in DMF. The peak of Pt arises from Pt film sputtered on the glass substrate.

electrocatalytic activity. (4) The prepared Pd/SWNT nanocomposite exhibits superior catalytic activity and stability toward the eletrooxidation of ethanol over the commercial Pd/C catalyst. In spite of the facts that some excellent methods have been previously developed for the preparation of Pd/SWNT nanocomposites and that some strategies have been proposed for the post-treatment of ICPs to form novel kinds of functional materials, the strategy demonstrated in this study based on the electrochemical post-treatment of ICPs for the formation of ultrasmall, narrow size-distributed, and highly dispersed Pd nanoparticles supported by SWNTs has not been reported so far.

2. EXPERIMENTAL SECTION

2.1. Chemicals. 4-Formylbenzoic acid and 4-amino-3-hydroxybenzoic acid, $Zn(CH_3COO)_2$, and $Pd(CH_3COO)_2$ were all purchased from Sigma Aldrich. All solvents were purchased from Beijing Chemical Company (Beijing, China) and used without further purification. Aqueous solutions were prepared with Milli-Q water (Millipore, 18.2 MΩ·cm).

2.2. Synthesis of ZMP and Pd/SWNT Nanocomposite. The organic ligand, that is, metallo Schiff base (MSB), was synthesized by mixing 4-formylbenzoic acid (1.0 g, 6.7 mmol) and 4-amino-3-hydroxybenzoic acid (1.1 g, 7.3 mmol) into 40 mL of ethanol and the mixture was then refluxed for 30 min to form precipitate. The precipitate was first isolated by filtration and then washed with hot ethanol for at least three times and finally dried under vacuum at 60 °C (~70% yield) (Scheme 1 A-1). The structure of the synthesized MSB precipitate was confirmed by ^{1}H NMR (400 MHz, DMSO-d_6, δ): 12.99 (s, 2H), 9.57 (s, 1H), 8.78 (s, 1H), 8.12 (d, 2H), 8.07 (d, 2H), 7.48 (s, 1H), 7.44 (d, 1H), 7.23 (d, 1H).

To synthesize Zn-MSB-Zn ICP, MSB (60.0 mg, 0.22 mmol) and $Zn(OAc)_2$ (100.0 mg, 0.53 mmol) were mixed into 10 mL of dimethyl sulfoxide (DMSO). A 10 mL of diethyl ether was allowed to slowly diffuse into the mixture. After 30 min, yellow precipitate was formed. The as-formed precipitate was isolated and washed with DMSO and ethanol via centrifugation/redispersion cycles for at least three times. Each successive supernatant was decanted and replaced with fresh solvent. The precipitate was dried under vacuum at 60 °C to give Zn-MSB-Zn ICP as a yellow product (~45% yield) (Scheme 1 A-2). To synthesize the Zn-MSB-Pd precursor through an ion-exchange reaction, Zn-MSB-Zn ICP (8.0 mg, 0.019 mmol) was added into a DMF (1.0 mL) solution of $Pd(OAc)_2{\cdot}H_2O$ (4.48 mg, 0.020 mmol) through continuously shaking on a vortex mixer at room temperature for 2 h. During this process, the color of the mixture gradually changed from yellow to brown. The product was isolated and subsequently washed with fresh DMF for at least three times to give Zn-MSB-Pd (ZMP) ICP as a brown product (Scheme 1 A-3). In this process, a slightly excessive amount of Pd^{2+} was added into the mixture to ensure the complete replacement of Zn^{2+} coordinated with Schiff base moieties within the Zn-MSB-Zn ICP (Scheme 1 A-3).

To obtain the ZMP/SWNT nanocomposite, the synthesized ZMP ICP (5 mg) and SWNTs (10 mg) were added into 1 mL of DMF and the resulting mixture was stirred vigorously for 2 h under ambient temperature. The product was washed carefully by DMF for several times. After being dried under vacuum, 3.14 mg ZMP/SWNT nanocomposite was dispersed in 0.5 mL of DMF to form a homogeneous dispersion under ultrasonication. To carry out the electrochemical post-treatment of ZMP ICP to form the Pd/SWNT nanocomposite, 10 μL of the ZMP/SWNT dispersion in DMF was drop-coated onto glassy carbon (GC) electrode (3 mm in diameter). The electrode was first dried at ambient temperature to evaporate the solvent and then polarized at the potential of −0.2 V for 600 s in 0.5 M H_2SO_4 solution. In this case, a three-electrode electrochemical cell was used for the electrochemical post-treatment of ZMP ICP with the ZMP/SWNT-modified GC electrode as working electrode, a platinum spiral wire as counter electrode, and a Ag/AgCl electrode (KCl-

saturated) as reference electrode. The electrochemical post-treatment of ZMP ICP was performed at room temperature.

Scanning electron microscopy (SEM) was performed on S-4800 (Hitachi, Japan), and energy-dispersive X-ray (EDX) analysis was performed on an EDAX detector on SEM. Transmission electron microscopy (TEM) was performed on a JEOL JEM-2011 (100 kV). The composition was determined by X-ray photoelectron spectroscope (XPS) (ESCALab220i-XL electron spectrometer, 300W Al KR radiation). For SEM and XPS characterization, indium−tin oxide (ITO) and glassy carbon slides were used as the substrate for the electrochemical postpretreatment, respectively.

2.3. Electrochemistry. Cyclic voltammetry used to characterize the hydrogen adsorption/desorption processes on the as-formed Pd/SWNT nanocomposite and the commercial Pd/C catalyst was performed in a N_2-saturated H_2SO_4 solution (0.5 M) at the scan rate of 50 $mV{\cdot}s^{-1}$. Cyclic voltammetry for characterizing the oxidation of ethanol was carried out in 0.10 M NaOH solution containing 0.10 M ethanol. The stability for the electrocatalytic oxidation of ethanol was evaluated by amperometric $I-t$ measurements in 0.10 M NaOH at −0.30 V. For comparison, commercial Pd/C catalyst was examined with respect to its electrocatalytic activity toward the ethanol oxidation and the stability for the electrocatalysis under the same conditions employed for the as-formed Pd/SWNT nanocomposite. For such a purpose, 10 mg commercial Pd/C catalyst was dispersed in 0.5 mL of DMF to form a homogeneous dispersion under ultrasonication. Then, 10 μL of the dispersion was drop-coated onto GC electrode, and the electrode (i.e., Pd/C-modified electrode) was dried under ambient temperature to evaporate the solvent. All electrochemical experiments were performed on an electrochemical workstation (CHI 650D, Shanghai, China).

3. RESULTS AND DISCUSSION

3.1. Formation of Pd-Based ZMP ICP. To prepare Pd nanoparticles supported by SWNTs, Zn-MSB-Pd (ZMP) ICP was synthesized as the precursor ICP. For the synthesis of ZMP ICP, Zn-MSB-Zn (ZMZ) ICP was first synthesized through the coordination chemistry between zinc acetate and metallo-Schiff base (MSB) as described in Experimental Section.[35] As shown in Scheme 1 A (2), the repeating unit of ZMZ ICP was formed with one Zn^{2+} coordinated with two carboxylate groups from two neighboring Schiff base ligands, while a second Zn^{2+} coordinated with the hydroxyl group and amine group within the same unit of the tridentate Schiff base ligand. Figure 1 A shows SEM image of the as-obtained ZMZ ICP that exhibits a spherical shape with a diameter of (100 ± 37) nm. The featureless diffraction peaks indicates that the as-formed ZMZ ICP is amorphous and not crystalline (data not shown), suggesting that the ZMZ is one kind of ICPs.[36] Then, ZMP ICP was prepared through a controlled ion-exchange approach by mixing ZMZ ICP and $Pd(OAC)_2$ into DMF and shaking the resulting mixture for 2 h at ambient conditions. During this process, Zn^{2+} coordinated with the hydroxyl group and amine group within the same unit was readily replaced by Pd^{2+} ions to form ZMP ICP, but the Zn^{2+} coordinated with two carboxylate sites from two neighboring units cannot be replaced (Scheme 1 A (3)). This ion-exchange process could also be easily observed with naked eye because during this process the solution color changed from yellow (Zn-MSB-Zn) to brown (Zn-MSB-Pd). Figure 1 B displays SEM image of the as-formed ZMP ICP. The ion-exchange reaction does not lead to an obvious change of either the size or the shape of ICP particles. TEM image (Figure 1 C) further confirms that ZMP ICP also exhibits sphere-like morphology with a size of ca. 100 nm and a smooth surface. The composition of the resulting ZMP ICP was determined using energy dispersive X-ray (EDX) spectroscopy (Figure 1 D) and the presence of C, N, O, Zn, and Pd elements further confirms the formation of the ZMP ICP, in which the peaks of C, N, O, Zn, and Pd elements arise from ZMP ICP, and the peak of Pt arises from Pt film sputtered on the glass substrate. The atom contents for Zn and Pd in the synthesized ZMP ICP was calculated to be 7.20% and 6.73% (~1:1, mole ratio), respectively, consistent with our proposed ion exchange mechanism (Scheme 1 A (3)). This result also reveals that the Zn^{2+} coordinated with the hydroxyl group and amine group within the same unit of tridentate Schiff base ligand was almost completely replaced by Pd^{2+}. Besides, the ion-exchange reaction proceeds rather fast with high conversion efficiency under the experimental conditions employed here.

3.2. Electrochemical Post-Treatment of ZMP ICP to Form Pd/SWNT Nanocomposite. To disperse Pd nanoparticles onto SWNTs, the as-synthesized ZMP ICP was first mixed with SWNTs to form ZMP/SWNT nanocomposite (Scheme 1 B). Interestingly, we found that the solubility of SWNTs was greatly improved after mixing with ZMP ICP. As could be seen from the photographs in Figure 2 A, the as-synthesized ZMP ICP gives a brown homogeneous dispersion in DMF, while the pristine SWNTs were found to precipitate at the bottom of the bottle within a short time (typically after two hours). However, after mixing ZMP ICP into the dispersion of SWNTs in DMF, SWNTs were well solubilized to give a homogeneous dispersion that was found to be stable for at least one week. This phenomenon could be presumably explained by the noncovalent interactions between ZMP ICP and SWNTs. For instance, ZMP ICP may bind to SWNTs through $\pi-\pi$ stacking between the aromatic bases of organic ligand and graphite surface of SWNTs.[37] Moreover, the uncoordinated carbonyl groups in the ZMP ICP are also likely to interact with the free oxygen-containing groups on the surfaces of SWNTs.[38] These interactions could make ZMP ICP evenly adsorb onto SWNTs. As displayed in Figure 2 B, SWNTs were uniformly covered by ZMP ICP nanoparticles and the nanoparticles almost maintained their original size and spherical shape on the SWNT surface. Such a property was beneficial to the formation of ultrasmall and highly dispersed Pd nanoparticles onto

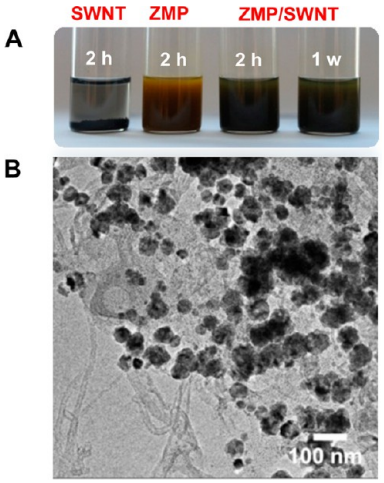

Figure 2. (A) Photographs of pristine SWNTs, ZMP ICP, and ZMP/SWNT dispersions in DMF. The photographs were taken after the dispersions were allowed to stand by for different lengths of time as indicated in the figure. (B) TEM image of the ZMP/SWNT nanocomposite.

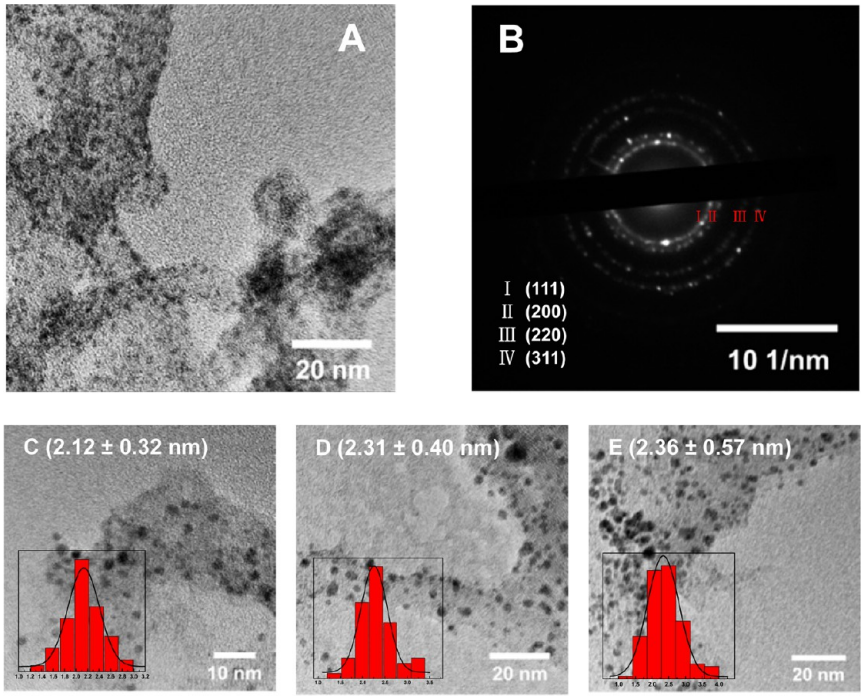

Figure 3. (A) TEM image and (B) selected area electron diffraction (SAED) of the as-formed Pd/SWNT by electrochemical post-treatment at the potential of −0.2 V for 600 s. The particle size distribution histograms of the Pd/SWNT nanocomposites formed by the electrochemical post-treament of different lengths of time of (C) 600, (D) 1200, and (E) 2400 s, at the potential of −0.2 V in 0.5 M H_2SO_4.

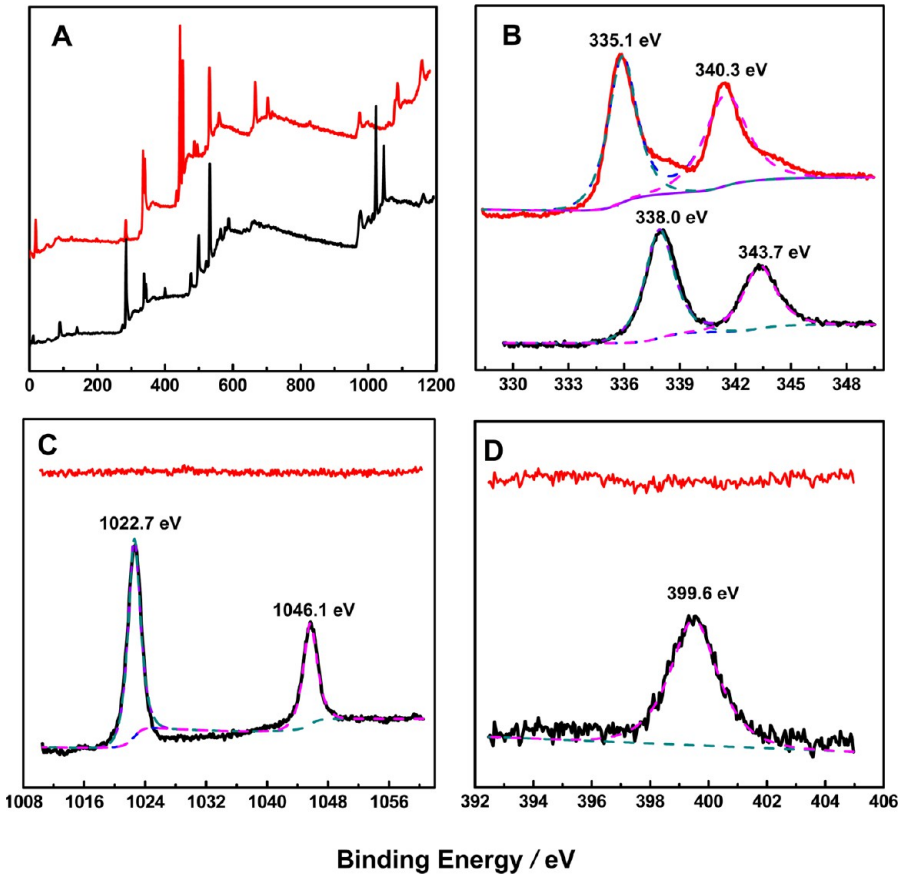

Figure 4. X-ray photoelectronic spectroscopy (XPS) of ZMP/SWNT (black lines) and the Pd/SWNT (red lines) formed by electrochemical post-treatment at a potential of −0.2 V for 600 s. (A) Full spectrum, (B) Pd3d peaks, (C) Zn2p peaks, and (D) N1s peaks.

dx.doi.org/10.1021/am403996d | *ACS Appl. Mater. Interfaces* 2013, 5, 11471−11478

SWNTs through the electrochemical post-treatment of ZMP ICP, as demonstrated below.

The electrochemical post-treatment was carried out by polarizing the ZMP/SWNT-modified glassy carbon electrode at the potential of −0.2 V for 600 s in 0.5 M H_2SO_4. After electrochemical post-treatment, Pd nanoparticles were highly dispersed on the surface of SWNTs, as could be seen from the TEM image in Figure 3 A. The histograms of Pd nanoparticles size (Figure 3 C) show that Pd nanoparticles supported by SWNTs have a narrow size distribution with a peak centered at ca. 2.1 nm (2.12 ± 0.32 nm). The selected area electron diffraction (SAED) in Figure 3 B further confirms the presence of Pd in the Pd/SWNT nanocomposite and the presence of continuous rings could be indexed to palladium's (111), (200), (220), and (311) planes, characteristic of the crystalline Pd face centered cubic pattern.[39] To further demonstrate the effect of electrochemical post-treatment on the formation of the Pd/SWNT nanocomposite, we conducted the post-treatment with different times of 600, 1200, and 2400 s. Interestingly, we found that the size of Pd nanoparticles does not vary obviously with the times employed here, as shown in Figure 3 C−E. The mean sizes of the as-synthesized Pd nanoparticles were 2.12 ± 0.32, 2.31 ± 0.40, and 2.36 ± 0.57 nm after the electrodes were polarized for 600, 1200, and 2400 s, respectively. This is different from the electrochemical deposition, in which the size of the as-deposited metal nanoparticles always grow larger as the deposition time increases, resulting in difficulty in obtaining uniform and small size materials. The independence of the Pd nanoparticles size on the post-treatment time observed in our study suggests that the ZMP ICP plays important roles in the formation of Pd nanoparticles; ZMP ICP provides uniform sites for confining the metal precursor Pd^{2+} ions by the coordination interaction between Pd^{2+} ions and the Schiff base, and tends to evenly absorb onto SWNTs to form a three-dimensional network, as mentioned above. These features could eventually result in the formation of ultrasmall and highly dispersed Pd nanoparticles onto SWNTs when the ZMP ICP was subject to the electrochemical post-treatment.

We shall note that, different from the earlier attempts to prepare Pd nanoparticles with stabilizers, in which the stabilizers could not be totally removed from the as-formed nanoparticles, which results in low electrocatalytic activity of Pd nanoparticles,[40] ZMP ICP precursors can completely decompose into the solution without remaining on the surface of as-formed Pd/SWNT during post-treatment process. This is proved by X-ray photoelectron spectroscopy (XPS). As depicted in Figure 4 B, before the electrochemical post-treatment, the ZMP/SWNT nanocomposite displays Pd 3d peaks at 338.0 and 343.7 eV (black curve), revealing the existence of Pd^{2+} in the nanocomposite. After the electrochemical post-treatment, the as-formed nanocomposite exhibits Pd 3d peaks at 335.1 and 340.3 eV, suggesting the formation of Pd^0 nanoparticles.[41] Meanwhile, the post-treatment essentially leads to the disappearance of Zn 2p peaks (1022.7 and 1046.1 eV, Figure 4 C) and N 1s peak (399.6 eV, Figure 4 D) in the ZMP/SWNT nanocomposite, implying that no detectable ZMP ICP was remained on the as-formed Pd/SWNT nanocomposite.[42] This may be attributed to the poor stability of ZMP ICP in 0.5 M H_2SO_4 solution; when the ZMP/SWNT-modified electrode was immersed into 0.5 M H_2SO_4 solution, the ZMP ICP tended to decompose slowly through the hydrolysis of C═N double bond, and at the same time the coordinated Pd^{2+} ions were reduced to Pd^0 nanoparticles, leaving the protonated MSB ligand dissolved into the electrolyte.

While some methods have so far been demonstrated for the formation of Pd nanoparticles, the method described here remains remarkable in terms of its experimental conditions employed and the excellent properties of the as-formed nanoparticles. For example, chemical vapor deposition method and hydrothermal method generally suffer from the need for a complex synthetic procedure, sophisticated equipment, and critical conditions such as high pressure or temperature (Table 1).[33−35] Microemulsion method, intermittent microwave heating method and surfactant self-reduction method normally utilize organic solvents or surfactants to prevent the spontaneous absorption of Pd nanoparticles at the defects or the edges on SWNTs in the reduction process.[36−38] Moreover, the size of Pd nanoparticles prepared with most of the existing methods was larger than that of the nanoparticles prepared in this study.[43−48] As described above, our method demonstrated here is simple, surfactant-free, and no need for critical experimental conditions. Moreover, the as-synthesized Pd nanoparticles supported by SWNTs have small size, narrow size distribution and high dispersion on SWNTs. These properties substantially endow the as-prepared Pd/SWNT nanocomposite with excellent electrocatalytic activity toward the oxidation of ethanol, as demonstrated below.

Table 1. Comparison of the Methods Reported for the Preparation of the Pd/SWNT

methods	sizes of Pd NPs (nm)	conditions	refs
chemical reduction	4−25	(1) pretreatment of CNTs, (2) Reductant such as H_2, $NaBH_4$ and so on, and (3) Stabilizer	18, 19, 37
atomic layer deposition	1−5	(1) expensive precursors and (2) expensive equipment	44
IMH method	3−10	complicated procedures	45
chemical fluid deposition	2−10	usage of super critical CO_2 fluids	46
seed-mediated growth	3−50	largely related to the precursors	47
surfactant-free method	3−30	careful choice of intermediate or template	13−17
nonselective electrodeposition	5−20	(1) strictly control the deposition parameters and (2) modification of CNTs	48
electrochemical post-treatment	**2−3**	**green and stabilizer-free**	**our method**

3.3. Electrochemical Catalytic Activity of Pd/SWNT toward Ethanol Oxidation. To evaluate the catalytic behavior of the as-prepared Pd/SWNT nanocomposite toward the electrooxidation of ethanol, cyclic voltammetry was conducted in 0.10 M NaOH solution containing 0.10 M ethanol with the Pd/SWNT-modified GC electrode as working electrode. For comparison, commercial Pd/C catalyst was also defined onto GC electrode and the electrode (i.e., Pd/C-modified electrode) was used as working electrode for cyclic voltammetric measurements. The electrochemically active specific surface area (ECSA) was calculated by the charge involved in the hydrogen adsorption/desorption process in terms of following equation[3]

$$\mathrm{ECSA} = Q_H/(0.21 \times m_{Pd})$$

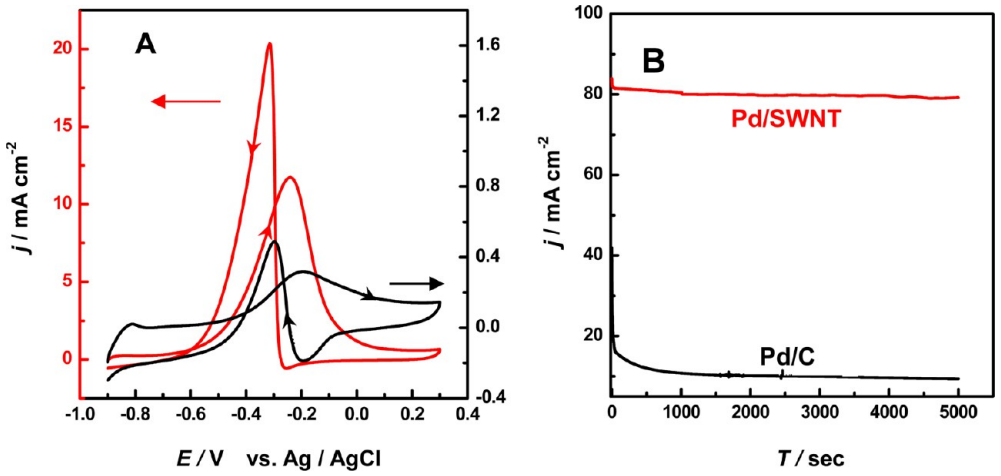

Figure 5. (A) Cyclic voltammograms obtained at the Pd/SWNT-modified electrode (red curve) and the commercial Pd/C-modified electrode (black curve) in 0.10 M NaOH containing 0.10 M ethanol. Scan rate, 50 mV s^{-1}. (B) Current−time curves recorded at the Pd/SWNT-modified (red curve) and commercial Pd/C-modified (black curve) electrodes in 0.10 M NaOH containing 0.10 M ethanol at −0.3 V.

where, Q_H (mC) is the charge of hydrogen adsorption/desorption. The constant of 0.21 ($mC \cdot cm^{-2}$) represents the specific electrical charge associated with monolayer adsorption of hydrogen on Pd, and m_{Pd} is the amount of Pd loaded on an electrode which was calculated by the mass fraction of Pd in ZMP ICP (i.e., 23.7%) and in Pd/C (i.e., 10%). The ECSA of Pd/SWNT was calculated to be 3.81 $m^2 \cdot g^{-1}$, which was 15 times higher than that of the commercial Pd/C (0.25 $m^2 \cdot g^{-1}$). This indicates that Pd/SWNT possesses a much higher ECSA and promotes atom utilization of Pd on SWNTs. Such a property essentially ensures the excellent electrocatalytic activity of the as-prepared Pd/SWNT nanocomposite toward the oxidation of ethanol. Figure 5 A compares typical cyclic voltammograms of the oxidation of ethanol on the Pd/SWNT-modified and the commercial Pd/C-modified electrodes. At the Pd/SWNT-modified electrode, the oxidation of ethanol commences at −0.60 V (red curve), which was −200 mV more negative than that at the commercial Pd/C-modified electrode (black curve). Moreover, the maximum current density for the oxidation of ethanol in the positive-going potential scan at the Pd/SWNT-modified electrode (red curve) was 10 times higher than that at the commercial Pd/C-modified electrode (black curve). This comparison strongly suggests the Pd/SWNT nanocomposite possesses an enhanced electrocatalytic activity toward ethanol oxidation compared with the commercial Pd/C catalyst. Furthermore, we found that the as-prepared Pd/SWNT nanocomposite was quite stable for the ethanol oxidation, as shown in Figure 5 B. For the oxidation of ethanol, the Pd/SWNT-modified electrode shows a steady-state current density of ∼81.7 $\mu A\ cm^{-2}$ and only 5% decrease was recorded after continuously running the measurements for 5000 s. In contrast, the commercial Pd/C-modified electrode exhibits an initial current density of ∼40.2 $\mu A\ cm^{-2}$ which decreases rapidly to 5.7 $\mu A\ cm^{-2}$ in 600 s. These results demonstrate that the as-prepared Pd/SWNT nanocomposite possesses a high electrocatalytic activity and stability for the oxidation of ethanol, suggesting its potential applications in direct ethanol fuel cells.

4. CONCLUSIONS

In summary, we have demonstrated a novel method for preparing SWNTs supported Pd nanoparticles by electrochemical post-treatment of Zn-MSB-Pd infinite coordinate polymers. In comparison with the existing methods, this strategy is facile, surfactant-free, and no need for complex synthetic procedures or sophisticated equipment. Moroever, the as-synthesized Pd nanoparticles possess small size, high dispersion and narrow size distribution. Electrochemical investigations demonstrate that the as-formed Pd/SWNT nanocomposite exhibits much higher electrocatalytic activity and stability toward the ethanol oxidation than the commercial Pd/C catalyst, suggesting the promising application of the Pd/SWNT nanocomposite prepared in this study in fuel cells. This study not only provides a new avenue to the preparation of Pd/SWNT catalyst for fuel cells but also broadens the post-treatment of infinite coordination polymers to form novel kinds of functional materials through an electrochemical mechanism.

AUTHOR INFORMATION

Corresponding Author

*E-mail: lqmao@iccas.ac.cn. Fax: +86-10-62559373.

Notes

The authors declare no competing financial interest.

ACKNOWLEDGMENTS

We acknowledge financial support from the National Natural Science Foundation of China (Grants 21321003, 20935005, 21127901, 21210007, and 91213305 for L.M. and 21175141 for L.Y.), the National Basic Research Program of China (973 program, 2010CB33502, 2013CB933704), and The Chinese Academy of Sciences (KJCX2-YW-W25).

REFERENCES

(1) Claudio, B.; Pei, K. *Chem. Rev.* **2009**, *109*, 4183−4206.
(2) Wang, A.; Xu, H.; Feng, J.; Ding, L.-X.; Tong, Y.-X.; Li, G.-R. *J. Am. Chem. Soc.* **2013**, *135*, 10703−10709.
(3) Tian, N.; Zhou, Z.; Yu, N.; Wang, L.; Sun, S. *J. Am. Chem. Soc.* **2010**, *132*, 7580−7581.
(4) Chun, L.; Kariate, S.; Hsin, L.; Ja-an, A.; Michael, H. *J. Am. Chem. Soc.* **2010**, *132*, 14546−14553.
(5) Liang, W.; Yoshihiro, N.; Yusuke, Y. *J. Am. Chem. Soc.* **2011**, *133*, 9674−9677.
(6) Chen, X.; Wu, G.; Chen, J.; Chen, X.; Xie, Z.; Wang, X. *J. Am. Chem. Soc.* **2011**, *133*, 3693−3695.

(7) Lee, K.; Kang, S.; Lee, S.-U.; Park, K.-H.; Lee, Y.; Han, S. *ACS Appl. Mater. Interfaces* **2012**, *4*, 4208−4214.
(8) Irina, B.; Valentina, G.; Valentin, Y.; Lyudmila, M. *J. Mater. Chem.* **2012**, *22*, 6441−6448.
(9) Jun, Y.; Ying, X.; Rui, H.; Bao, J.; Hong, G. *ACS Appl. Mater. Interfaces* **2013**, *5*, 6571−6579.
(10) Jun, H.; William, W.; Hae, W.; Chan, Y.; Allan, J.; Lee, T. *ACS Appl. Mater. Interfaces* **2009**, *1*, 1063−6579.
(11) Gong, K.; Chakrabarti, S.; Dai, L. *Angew. Chem., Int. Ed.* **2008**, *47*, 5446−5450.
(12) Qu, L.; Dai, L.; Osawa, E. *J. Am. Chem. Soc.* **2006**, *128*, 5523−5532.
(13) Maschmann, M.; Franklin, A.; Scott, A.; Janes, D.; Sands, T.; Fisher, T. *Nano Lett.* **2006**, *6*, 2712−2717.
(14) Qu, L.; Dai, L. *J. Am. Chem. Soc.* **2005**, *127*, 10806−10807.
(15) Khalap, V.; Sheps, T.; Kane, A.; Collins, P. *Nano Lett.* **2010**, *10*, 896−901.
(16) Wu, K.; Mao, X.; Liang, Y.; Chen, Y.; Tang, Y.; Zhou, Y.; Lin, J.; Ma, C.; Lu, T. *J. Power Sources* **2008**, *219*, 258−262.
(17) Hu, F.; Shen, P.; Li, Y.; Liang, J.; Wu, J.; Bao, Q.; Li, C.; Wei, Z. D. *Fuel Cells* **2008**, *8*, 429−432.
(18) Li, S.; Dong, Z.; Yang, H.; Guo, S.; Gou, G.; Ren, R.; Zhu, Z.; Jin, J.; Ma, J. *Chem.—Eur. J.* **2013**, *19*, 2384−2391.
(19) Li, H.; Han, L.; Cooper-White, J. *Green Chem.* **2012**, *14*, 586.
(20) Halder, A.; Sharma, S.; Hegde, M. S.; Ravishankar, N. *J. Phys. Chem. C.* **2009**, *113*, 1466−1473.
(21) Koenigsmann, C.; Santulli, A.; Gong, K.; Zhou, W.; Sutter, E.; Wong, S.; Adzic, R. *J. Am. Chem. Soc.* **2011**, *133*, 9783−9795.
(22) Erikson, H.; Sarapuu, Ave.; Tammeveski, K.; Gullónb, J. S.; Feliub, J. M. *Electrochem. Commun.* **2011**, *13*, 734−737.
(23) Crane, E.; Girolami, G.; Nuzzo, R. *Acc. Chem. Res.* **2000**, *33*, 869−877.
(24) Yan, S.; Maeda, H.; Kusakabe, K.; Morooka, S. *Ind. Eng. Chem. Res.* **1994**, *33*, 616−622.
(25) Wang, Y.; Xie, S. F.; Liu, J.; Park, J.; Huang, C.; Xia, Y. *Nano Lett.* **2013**, *13*, 2276−2281.
(26) Oh, M.; Mirkin, C. A. *Nature* **2005**, *438*, 651−654.
(27) Kuwabara, J.; Stern, C.; Mirkin, C. *J. Am. Chem. Soc.* **2007**, *129*, 10074−10075.
(28) Cho, W.; Lee, H.; Oh, M. *J. Am. Chem. Soc.* **2008**, *130*, 16943−16946.
(29) Kang, L.; Fu, H.; Cao, X. Q.; Shi, Q.; Yao, J. *J. Am. Chem. Soc.* **2011**, *133*, 1895−1901.
(30) Lee, H.; Cho, W.; Jung, S.; Oh, M. *Adv. Mater.* **2009**, *21*, 674−677.
(31) Yang, C.-X.; Ren, H.-B.; Yan, X.-P. *Anal. Chem.* **2013**, *85*, 7441−7446.
(32) Jung, S.; Cho, W.; Lee, H.; Oh, M. *Angew. Chem., Int. Ed.* **2009**, *48*, 1459−1462.
(33) Liu, X. *Angew. Chem., Int. Ed.* **2009**, *48*, 3018−3021.
(34) Huang, P.; Jiang, Q.; Yu, P.; Yang, L. F.; Mao, L. *ACS Appl. Mater. Interfaces* **2013**, *5*, 5239−5246.
(35) Cho, W.; Lee, Y. H.; Lee, H. J.; Oh, M. *Adv. Mater.* **2011**, *23*, 1−4.
(36) Spokoyny, A.; Kim, D.; Sumrein, A.; Mirkin, C. *Chem. Soc. Rev.* **2009**, *38*, 1218−1227.
(37) Zhang, L.; Guo, C.; Cui, Z.; Guo, J.; Dong, Z.; Li, C. *Chem.—Eur. J.* **2012**, *18*, 15693−15698.
(38) Pan, Y.; Ma, D.; Liu, H.; Wu, H.; He, D.; Li, Y. *J. Mater. Chem.* **2012**, *22*, 10834−10839.
(39) Huang, X.; Tang, S.; Zhang, H. H.; Zhou, Z. Y.; Zheng, N. F. *J. Am. Chem. Soc.* **2009**, *131*, 13916−13917.
(40) Qin, Y.; Zhang, X.; Wang, J.; Wang, L. *J. Mater. Chem.* **2012**, *22*, 14861−14863.
(41) Paredis, K.; Ono, L.; Behafarid, F.; Zhang, Z.; Yang, J.; Frenkel, A.; Cuenya, B. *J. Am. Chem. Soc.* **2011**, *133*, 13455−13464.
(42) Moulder, J.; Stickle, W.; Sobol, P.; Bomben, K. *Handbook of X-Ray Photoelectron Spectroscopy*, 2nd ed.; Physical Electronics, Inc.: Chanhassen, MN, 1992.
(43) Yang, C. W.; Chanda, K.; Lin, P. H.; Wang, Y. N.; Liao, C. W.; Huang, M. H. *J. Am. Chem. Soc.* **2011**, *133*, 19993−20000.
(44) Sairanen, E.; Karinen, R.; Borghei, M.; Kauppinen, E. I.; Lehtonen, J. *ChemCatChem* **2012**, *4*, 2055−2061.
(45) Zheng, H. T.; Li, Y. l.; Chen, S. X.; Shen, P. K. *J. Power Sources* **2006**, *163*, 371−375.
(46) Lin, Y. H.; Cui, X. L.; Ye, X. R. *Electrochem. Commun.* **2005**, *7*, 267−274.
(47) Zhang, W. J.; Baia, L.; Lua, L. M.; Chen, Z. *Colloids Surf. B.* **2012**, *97*, 145−149.
(48) Day, T. M.; Unwin, P. R.; Macpherson, J. V. *Nano Lett.* **2007**, *7*, 51−57.